Water Practice & Technology

IWA PUBLISHING

Water Practice & Technology Vol 19 No 4, 1162 doi: 10.2166/wpt.2024.051

Assessment and modeling of mercury adsorption on carbon-based adsorbents prepared from *Jacaranda mimosifolia* and guava biomass via pyrolysis and hydrothermal carbonization

Víctor Aljair Morales-Herrera[a], Fátima Gisela Quintero-Álvarez[b], Didilia Ileana Mendoza-Castillo[b,c,*], Hilda Elizabeth Reynel-Ávila[b,c], Ismael Alejandro Aguayo-Villarreal[d], Verónica Janeth Landin-Sandoval[a] and Adrián Bonilla-Petriciolet[b]

[a] Universidad Tecnológica Metropolitana de Aguascalientes, Aguascalientes, Mexico
[b] Instituto Tecnológico de Aguascalientes, Aguascalientes, Mexico
[c] Consejo Nacional de Humanidades, Ciencias y Tecnologías, Ciudad de Mexico, Mexico
[d] Universidad de Colima, Colima, Mexico
*Corresponding author. E-mail: dimendozaca@conahcyt.mx

FGQÁ, 0000-0001-5602-5678; DIMC, 0000-0002-8047-9116; HERÁ, 0000-0002-4102-2252; IAAV, 0000-0002-7134-1692; ABP, 0000-0002-0197-3539

ABSTRACT

The mercury adsorption properties of carbon-based materials prepared from jacaranda (*Jacaranda mimosifolia*) and guava (*Psidium guajava*) seed wastes are reported and compared in this paper. These adsorbent samples were obtained via pyrolysis and hydrothermal carbonization. Mercury adsorption equilibrium was studied at pH 4 and 20–40 °C, and the adsorption enthalpy changes were calculated for all adsorbent samples. The results showed that jacaranda-based materials contained a higher amount of acidic functional groups than guava seed-based adsorbents, and consequently, their mercury adsorption properties were better. The surface area of these adsorbents was <10 m^2/g thus being classified as low-porosity materials. Elemental analysis indicated that all adsorbents were mainly composed of oxygen (4–25%) and carbon (75–95%). The calculated adsorption capacities at saturation of the best adsorbent were 18.05–30.09 mg/g under the tested experimental conditions. Statistical physics calculations also indicated that the adsorption mechanism of $HgCl_2$ species was multi-molecular and endothermic. Ligand exchange and van der Waals forces were involved in generating the mercury–adsorbent interface. These results highlight the importance of comparing and optimizing biomass thermochemical conversion routes to tailor the surface properties of adsorbents used for water purification.

Key words: biomass thermochemical conversion, guava seed-based adsorbents, heavy metal, jacaranda-based adsorbents, mercury adsorption, water depollution

HIGHLIGHTS

- Assessment and modeling of mercury adsorption.
- Mercury adsorption properties of carbon-based materials prepared from jacaranda (*Jacaranda mimosifolia*) and guava (*Psidium guajava*) seed wastes.
- Importance of comparing and optimizing biomass thermochemical conversion routes.

1. INTRODUCTION

The existence of dissolved mercury in water is caused by both natural and anthropogenic pollution sources where the residual discharge from various industries (e.g., mining, energy, battery manufacturing, aerospace, and textiles) plays a significant role in its environmental release (Velempini & Pillay 2019; Prasetya *et al.* 2020). This heavy metal is toxic and non-biodegradable, and its bioaccumulation in the environment can affect living organisms and pose a risk to public health (Prasetya *et al.* 2020; Li *et al.* 2021; He *et al.* 2023; Shukla *et al.* 2023; Zhang *et al.* 2023a). A chronic exposure to mercury has been associated to heart diseases, neurological damage, and cancer in humans (Velempini & Pillay 2019; Prasetya *et al.* 2020). Toxicological results using laboratory animals have also indicated that the mercury exposure can generate kidney damage, neuropathological effects, decrease

in fertility, besides showing carcinogenic activity; while growth retardation has been observed for plants exposed to mercury-polluted water (Syversen & Kaur 2012).

Effluents and wastewater containing mercury can be treated using various physicochemical methods including traditional coagulation and precipitation operations and advanced purification technologies such as membrane-based separation and electrochemical processes (Al-Jaaf *et al.* 2022; Ali *et al.* 2022a; Yoo *et al.* 2023). Particularly, the adsorption-based processes have proved to be effective for the removal of inorganic and organic pollutants from water. For example, Al-Jaaf *et al.* (2022) showed the benefits of using an eggplant peel-based adsorbent to purify a domestic wastewater. Therefore, the depollution of water containing mercury via adsorption is characterized by its lower cost and higher removal efficiency than those of other treatment technologies (Luo *et al.* 2020; Duman 2021; Jung *et al.* 2021). Zeolites, clay, polymers, industrial residues, activated carbons, chars, metal oxides, and their composites have been used as adsorbents to reduce the mercury concentrations in polluted streams (Zhu *et al.* 2012; Raji & Pakizeh 2014; Ganzagh *et al.* 2016; Saman *et al.* 2016; Shen *et al.* 2018; Prasetya *et al.* 2020; Jumah *et al.* 2021; Li *et al.* 2021; Liu *et al.* 2022; He *et al.* 2023). The performance of some of these materials is promising for large-scale water treatment due to their high adsorption capacities, but the main limitation is usually their depollution cost. The operational cost of adsorption systems is mainly related to the production of the solid phase used as the separation medium. Consequently, it is important to identify new feedstocks and low-cost and sustainable preparation routes to improve the economy of water treatment.

Adsorbents prepared by the thermochemical conversion of biomass wastes and subproducts are an interesting alternative for reducing the water purification cost associated with the mercury removal (Jung *et al.* 2021; Tran *et al.* 2021; Qin *et al.* 2023; Zhang *et al.* 2023a). Carbon-based adsorbents are typically obtained via the thermochemical conversion of biomass, in addition to surface functionalization, to tailor their surface properties. The adsorbent removal performance depends on the precursor feedstock, the synthesis route (e.g., temperature and dwell time), and the chemicals utilized in their functionalization. The quantity and type of adsorbent functional groups (i.e., active sites to bind the water pollutant) are determined by manipulating the synthesis parameters. Therefore, the analysis of the preparation conditions is crucial for establishing the final surface chemistry of the adsorbent.

Pyrolysis and hydrothermal carbonization are reliable biomass conversion routes to obtain materials to reduce the concentration of water pollutants, such as mercury (Correa *et al.* 2019; Zhang *et al.* 2023a). They differ in terms of energy consumption, process operating conditions, adsorbent yields, and final product properties (Rattanachueskul *et al.* 2017; Nguyen *et al.* 2022). The degradation of the natural polymers contained in biomass determines the development of the porous adsorbent structure and occurs at different temperatures for each preparation route. Therefore, adsorbents prepared from the same feedstock using hydrothermal carbonization and pyrolysis can differ substantially in their surface functionalities and textural properties (Zhang *et al.* 2023a). The tailoring of adsorbent properties implies the identification of the best biomass conversion conditions to improve the removal of the target adsorbate. Adsorbents for liquid-phase separation can be prepared via the pyrolysis and hydrothermal carbonization of biomass residues such as coconut shells (Jain *et al.* 2015), sugarcane bagasse (Rattanachueskul *et al.* 2017), tree leaves (Yang *et al.* 2019), palm kernel shells (Beri *et al.* 2021), rice husk (Jung *et al.* 2021), and corn straw (Zhang *et al.* 2023a). The porous solids synthesized from the conversion of lignocellulosic biomass residues typically contain oxygenated functional groups. Carboxylic, phenolic, lactonic, ketone, and hydroxyl groups are important for the mercury adsorption on carbon-based surfaces (Jain *et al.* 2015; Duman 2021; Nguyen *et al.* 2022). Consequently, it is important to compare the removal performance and properties of the adsorbents obtained using both hydrothermal carbonization and pyrolysis for the available variety of feedstock to identify the best alternative. However, this comparative approach has not been implemented in the preparation of carbon-based adsorbents in previous studies, which usually implies the definition of arbitrary adsorbent preparation conditions that are expected to be far from the optimum separation efficacy–cost balance.

A comparative analysis of the mercury removal properties of adsorbents obtained from pyrolysis and hydrothermal carbonization of *Jacaranda mimosifolia* fruit and guava (*Psidium guajava*; *Psidium guajava,* Linn) seeds is reported in this manuscript. Note that other studies have introduced these biomass wastes as feedstock to obtain activated carbons for the adsorption of pharmaceuticals, heavy metals, phenolic compounds, and dyes (Abdelwahab *et al.* 2007; Elizalde-González & Hernández-Montoya 2009; Treviño-Cordero *et al.* 2013; Anisuzzaman *et al.* 2016; Pezoti *et al.* 2016; Aly *et al.* 2019; Ortíz-Gutiérrez *et al.* 2020; Georgin *et al.* 2021; Ali *et al.* 2022b; Pindiga *et al.* 2022). For example, Elizalde-González & Hernández-Montoya (2009) used the

guava seeds as precursor of carbon-based adsorbents for the removal of acid dyes. Anisuzzaman *et al.* (2016) obtained activated carbon from guava seeds for chlorinated phenol adsorption. This biomass was also employed by Pezoti *et al.* (2016) as feedstock to prepare activated carbon for amoxicillin uptake. The guava biomass (including leaves, tree bark, and seeds) has also been applied as an adsorbent for the removal of arsenic, fluoride, heavy metals, phenol, and dyes (Domínguez & Serrano 2004; Abdelwahab *et al.* 2007; Valencia-Leal *et al.* 2012; Sánchez-Sánchez *et al.* 2013; Aly *et al.* 2019; Mohan *et al.* 2019; Mandal *et al.* 2020; Ortíz-Gutiérrez *et al.* 2020; Georgin *et al.* 2021; Ali *et al.* 2022b; Behera *et al.* 2022; Pindiga *et al.* 2022). Abdelwahab *et al.* (2007) and Ortíz-Gutiérrez *et al.* (2020) evaluated the performance of guava seeds for the adsorption of hexavalent chromium. Elizalde-González & Hernández-Montoya (2009) conducted experiments to assess the effectiveness of this residue as an adsorbent of different acid dyes. The guava leaves were employed for the removal of cadmium (Ali *et al.* 2022b; Pindiga *et al.* 2022), lead (Pindiga *et al.* 2022), and dyes (Aly *et al.* 2019). The adsorption of geogenic pollutants (e.g., arsenic and fluoride) using guava waste was also studied by Mohan *et al.* (2019), Behera *et al.* (2022), Sánchez-Sánchez *et al.* (2013) and Valencia-Leal *et al.* (2012). On the other hand, Mandal *et al.* (2020) reported the adsorption of phenol on guava tree bark. Regarding the *J. mimosifolia*, Treviño-Cordero *et al.* (2013), Georgin *et al.* (2021), and Domínguez & Serrano (2004) reported the synthesis of activated carbons using this biomass as precursor for the adsorption of heavy metals, dyes, and ketoprofen.

In this study, the application of the carbon-based materials prepared from these biomass wastes was extended to analyze the mercury removal at pH 4 and 25–40 °C. The main surface chemistry and textural parameters of these adsorbents were also studied and compared. Adsorption equilibrium was investigated using a statistical physics model to characterize the interactions involved in generating the interface responsible for mercury removal. Therefore, the aim of the present study was to assess the surface properties of these alternatives adsorbents to remove mercury from aqueous solutions. The novelty of this study lies on a reliable comparison and analysis of the application of pyrolysis and hydrothermal carbonization of residual biomass precursors to obtain new adsorbents for the removal of mercury as a priority water pollutant.

2. MATERIALS AND METHODS

2.1. Chemicals and analytical equipment

Deionized water (Mapla), analytical-grade $HgCl_2$ (Sigma-Aldrich), standard NaOH and HCl solutions (Fisher), and KBr (Sigma-Aldrich) were used in this study. The analytical equipment included: Empyrean (Malvern PANalytical) X-ray diffractometer, Nicolet iS10 (Thermo Scientific) FTIR spectrometer, TM3000 (Hitachi) scanning electron microscope with a coupled energy dispersive system (Nano XFlash, Bruker), ICE 3000 (Thermo Scientific) atomic absorption spectrophotometer and ASAP 2020 (Micromeritics) porosimeter.

2.2. Synthesis of carbon-based adsorbents using pyrolysis and hydrothermal carbonization and their physicochemical characterization

Carbon-based adsorbents were obtained from the biomass wastes of *J. mimosifolia* and *P. guajava* using pyrolysis and hydrothermal carbonization. These biomass wastes were obtained from local agri-food industries, parks, and gardens. They were then dried, shredded, and screened for the adsorbent synthesis. The pyrolysis of biomass waste was performed in a tubular furnace at 600 °C for 2 h with 10 °C/min heating rate under N_2 atmosphere. Hydrothermal carbonization was conducted in a 100-mL Teflon-lined autoclave reactor using a mass/volume ratio of 1:4 (i.e., 15 g of biomass and 60 mL of deionized water), at 180 °C for 12 h. The results reported in literature and preliminary trials were employed to define these preparation conditions. All adsorbents were washed with deionized water (until a constant pH was obtained from the residual effluent), dried in an oven for 24 h, and sieved to obtain a homogeneous particle size (~0.67 mm) for the adsorption studies. The samples were labelled as J-PYR, G-PYR, J-HTC, and G-HTC for the solid products obtained from the pyrolysis (PYR) and hydrothermal carbonization (HTC) of jacaranda (J) and guava seed (G) wastes, respectively. A schematic representation illustrating these experimental steps is reported in Supplementary material, Figure S1.

All the adsorbents were characterized to determine their main physicochemical properties. Specifically, the X-ray diffraction (XRD) patterns of these samples were obtained to analyze the crystalline structure and presence of inorganic elements. The adsorbents were analyzed at room temperature with Cu radiation ($\lambda = 1.5406$ Å) at 45 kV/40 mA in the angular range of 10°–60° 2θ. The functional groups present on the surfaces of these adsorbents were identified using Fourier transform infrared (FTIR) analysis. FTIR spectra of KBr-adsorbent pellets were recorded (32 scans per sample) in the 4,000–400 cm^{-1} range with a resolution of 4 cm^{-1}. The elemental

composition and morphology of all the adsorbents were determined by Scanning Electron Microscopy (SEM) with Energy Dispersive X-Ray (EDX) analysis. The samples were submitted to high vacuum with an accelerating voltage of 20 kV prior their analysis. Textural properties of adsorbent samples were estimated from N_2 physisorption, which were quantified at 77 K. Finally, the total basic and acidic groups were quantified according to the method described by Boehm (1994) and following the methodology reported by Pawlicka & Doczekalska (2013). The titrations were performed with 0.1 M NaOH and HCl solutions where the corresponding experimental conditions were 1 g/L of adsorbent/solution ratio, 48 h of contact time at 25 °C. Mass balance analysis was carried out with the results from solution titrations to calculate the concentrations of the adsorbent basic and acidic sites. The estimation of pH value of the point of zero charge (pH_{pzc}) for all the adsorbents was conducted following the methodology described by Milonjić *et al.* (1975).

2.3. Analysis of mercury adsorption equilibrium and isotherm modeling

The equilibrium of mercury adsorption on the four adsorbents (J-PYR, G-PYR, J-HTC and G-HTC) was studied with batch adsorbers. Adsorption studies were performed with initial mercury concentrations ($C_{ini,Hg}$) from 20 to 300 mg/L. Deionized water and $HgCl_2$ were utilized for the solution preparation. The experimental adsorption isotherms were obtained at a solution temperature of 20, 30, and 40 °C and pH 4 under constant stirring at 120 rpm for 24 h, with an adsorbent dose (w/V_{Hg}) of 5 g/L. The concentration of mercury dissolved in all the solutions was quantified via atomic absorption spectroscopy with a linear calibration curve. The adsorption capacities (q_{Hg}, mmol/g) of the carbon-based adsorbents were calculated with the mass balance

$$q_{Hg} = \left(\frac{C_{ini,Hg} - C_{eq,Hg}}{w}\right) V_{Hg} \tag{1}$$

where $C_{eq,Hg}$ is the equilibrium mercury concentration (mg/L), V_{Hg} is the mercury solution volume (L) and w is the adsorbent mass (g).

The experimental isotherms were utilized to estimate the mercury adsorption enthalpy change ($\Delta H°$, kJ/mol) using the van't Hoff approach and the procedure reported by Tran *et al.* (2017) and Lima *et al.* (2020) applying the next equations (Tran *et al.* 2017; Lima *et al.* 2020).

$$K_{Hg} = e^{\left[\frac{\Delta S^o}{R} - \frac{\Delta H^o}{R} \cdot \frac{1}{T}\right]} \tag{2}$$

$$K_{Hg} = \frac{\gamma_{Ads} C_{Ads,Hg}}{\gamma_e C_{eq,Hg}} \tag{3}$$

where $R = 8.314\text{E-}03$ kJ/K·mol is the universal gas constant, ΔS^o (kJ/K·mol) is the adsorption entropy change, K_{Hg} is the dimensionless thermodynamic equilibrium constant of the mercury adsorption on tested adsorbent at adsorption temperature T (K), $C_{Ads,Hg}$ is the concentration of mercury adsorbed on the adsorbent surface at the equilibrium (mg/L), γ_{Ads} and γ_e are the activity coefficients of mercury adsorbed on carbon-based surface and dissolved in the aqueous solution, respectively. Diluted solutions were assumed to obtain the K_{Hg} values for the $\Delta H°$ calculation following the approach suggested by Tran *et al.* (2017).

A statistical physics-based monolayer model (Amrhar *et al.* 2021) was applied to determine the steric parameters associated with mercury removal by the tested adsorbents. This statistical physics model was applied to interpret and understand the mercury adsorption mechanism. Several studies have proved that the adsorption models based on statistical physics fundaments are reliable to analyze the equilibrium adsorption data of water pollutant, thus overcoming the limitations of traditional adsorption models such as Freundlich and Langmuir equations (Sellaoui *et al.* 2019; Amrhar *et al.* 2021; Valdés-Rodríguez *et al.* 2022). This model was defined as (Amrhar *et al.* 2021)

$$q_{Hg} = \frac{n_{Hg} N_{Ads}}{1 + \left(\frac{C_{sm,Hg}}{C_{eq,Hg}}\right)^{n_{Hg}}} \tag{4}$$

where n_{Hg} is the number of adsorbed mercury species per adsorption site on the tested adsorbent, N_{Ads} is the

concentration of adsorption sites on the adsorbent surface that participate in mercury removal (mg/g), and $C_{sm,Hg}$ is the half-saturation mercury concentration (mg/L).

The model parameters were obtained from the nonlinear regression of experimental isotherms using the Excel® solver and the next objective function

$$F_{obj} = \sum_{i=1}^{n_{dat}} (q_{Hg,i}^{exp} - q_{Hg,i}^{cal})^2 + (q_{Hg,sat}^{exp} - q_{Hg,sat}^{cal})^2 \quad (5)$$

where n_{dat} is the number of experimental data points from each isotherm, *cal* and *exp* are the calculated (by the monolayer adsorption model) and experimental adsorption capacities (q_{Hg}, mg/g), and $q_{Hg,sat}$ is the mercury adsorption capacity at the adsorbent saturation condition (mg/g). This saturation adsorption capacity was defined as

$$q_{Hg,sat} = n_{Hg} \cdot N_{Ads} \quad (6)$$

Finally, the interaction energies ($\Delta E_{Hg\text{-}Ads}$, kJ/mol) for the mercury – adsorbent interface were calculated as follows (Amrhar *et al.* 2021)

$$\Delta E_{Hg-Ads} = RTln\left(\frac{S_{Hg}}{C_{sm,Hg}}\right) \quad (7)$$

where S_{Hg} (mg/L) is the $HgCl_2$ solubility in the aqueous solution.

3. RESULTS

3.1. Mercury adsorption and its modeling

The mercury adsorption isotherms obtained with J-HTC, G-HTC, J-PYR, and G-PYR are shown in Figure 1. The adsorbent yields obtained from the tested preparation routes were 26% (J-PYR), 24% (G-PYR), 73% (J-HTC), and 75% (G-HTC). These results confirmed the findings reported in other studies, where the yields of hydrothermal carbonization were higher than those of pyrolysis (Jian *et al.* 2018). The adsorption capacities of the adsorbents were 2.00 (± 0.01) – 17.05 (± 0.12), 0.60 (± 0.03) – 12.84 (± 0.57), 0.60 (± 0.02) – 30.69 (± 0.77) and 0.60 (± 0.03) – 10.23 (± 0.14) mg/g, respectively. These adsorption capacities corresponded to mercury removal percentages of 16–63, 15–72, 9–44 and 8–35% for J-HTC, J-PYR, G-HTC and G-PYR, respectively. J-PYR adsorbent exhibited the highest adsorption capacities, while G-PYR was outperformed by all the adsorbents. In fact, the adsorbent performance followed the trend: J-PYR >> J-HTC > G-HTC > G-PYR. These adsorption capacities increased by 84, 146, 77 and 127%, respectively, when the solution temperature changed from 20 to 40 °C. Mercury adsorption on these carbon-based materials was endothermic under tested experimental conditions. The calculated mercury adsorption enthalpies for J-HTC, G-HTC, J-PYR, and G-PYR were 25, 19, 40, and 39 kJ/mol, respectively. These $\Delta H°$ values indicated that the removal of this toxic heavy metal was governed mainly by physical intermolecular forces using these carbon-based adsorbents (Tran *et al.* 2020). The endothermic mercury adsorption on these materials was consistent with the findings reported by Yoo *et al.* (2023), Zabihi *et al.* (2010), Ismaiel *et al.* (2013), Park *et al.* (2019), Zúñiga-Muro *et al.* (2020), Valdés-Rodríguez *et al.* (2022), Gheitasi *et al.* (2022) and Kaveh & Bagherzadeh 2022. Hadi *et al.* (2015) reviewed the mercury adsorption on activated carbons and concluded that several studies have reported an endothermic process. Mercury adsorption enthalpy changes ranging from 9 to 39 kJ/mol have been reported for other activated carbons and adsorbents prepared from lignocellulosic biomass (Ismaiel *et al.* 2013; Gheitasi *et al.* 2022; Kaveh & Bagherzadeh 2022; Yoo *et al.* 2023). Therefore, these values agreed with the results of this study.

As indicated, the mercury adsorption properties of carbon-based adsorbents synthesized from jacaranda biomass were better than those of guava waste-based adsorbents, independent of the chosen preparation route (i.e., hydrothermal carbonization or pyrolysis). This performance may be related to the polymeric composition (i.e., lignin, hemicellulose, and cellulose) of these residues, which affects the adsorbent surface chemistry. Other studies have indicated that jacaranda biomass contains a polymeric fraction of 98% (i.e., cellulose 50%, hemicellulose 21%, and lignin 27%), whereas the polymeric content of guava seed biomass is 77% (i.e., cellulose 61%, hemicellulose 9%, and lignin 7%) (Elizalde-González & Hernández-Montoya 2009; Treviño-Cordero *et al.*

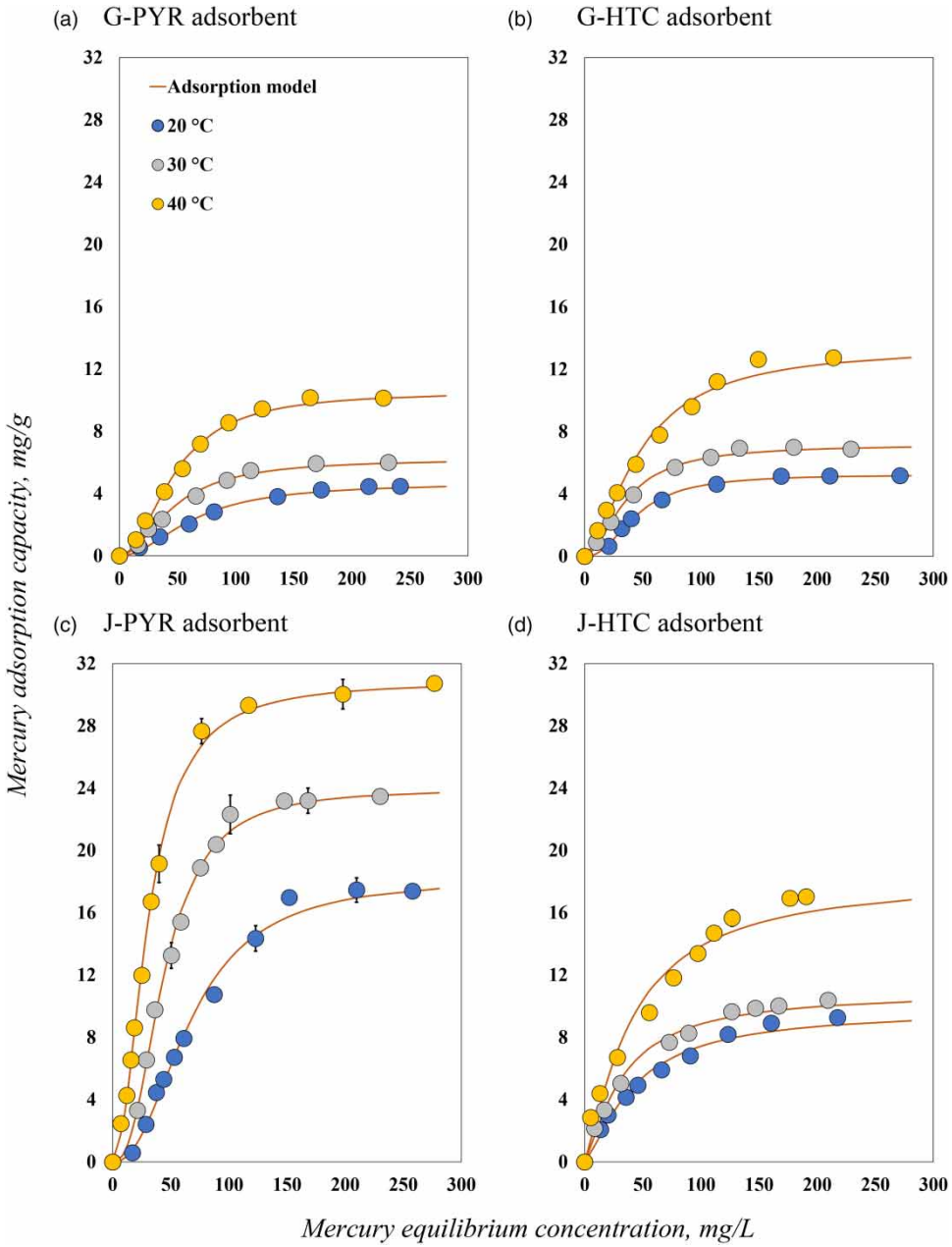

Figure 1 | Mercury adsorption isotherms at pH 4 using adsorbents obtained from the pyrolysis and hydrothermal carbonization of guava seed and jacaranda biomass.

2013). The type of thermal treatment applied to prepare each adsorbent also affects the presence of surface functionalities, because temperature promotes the degradation of natural polymers contained in the biomass precursor. Hemicellulose starts its thermal decomposition at ~160 °C, while lignin and cellulose begin to degrade at ~ 220 and 180 °C, respectively (Heidari *et al.* 2019). The degradation degree of these polymers depends on the adsorbent preparation process and its conditions (Heidari *et al.* 2019). Therefore, the type of biomass feedstock is a key parameter affecting the adsorption performance and physicochemical properties of carbon-based materials (Han *et al.* 2017). Note that the lignin content of the biomass precursor has been associated with a significant impact on the adsorbent surface chemistry, mainly on oxygenated functional groups (Arias-Arias *et al.* 2017). For instance, previous studies have shown that this polymer undergoes condensation reactions and polymerizes to form the adsorbent structure during hydrothermal carbonization of biomass (Plavniece *et al.* 2022). The jacaranda waste has a higher lignin content than guava seed residues, thus causing wetting and water diffusion inside the particles to become more constrained (Rodríguez-Correa *et al.* 2019). This may cause insoluble lignin to

generate a highly condensed adsorbent structure (Plavniece *et al.* 2022), which could limit the mass transfer of dissolved mercury in aqueous solutions, thus affecting the adsorption performance. Consequently, the J-PYR adsorbent sample obtained by pyrolysis exhibited a higher mercury adsorption capacity than J-HTC prepared via hydrothermal carbonization. Wang *et al.* (2022) also found similar results for the removal of cadmium ions with adsorbents prepared from Napier grass. Table 1 reports the concentrations of the acidic groups found in the tested adsorbent samples. The concentration of acidic sites followed the order: J-HTC > J-PYR ≅G-HTC > G-PYR. The jacaranda-based adsorbents had a higher concentration of oxygenated functionalities (e.g., hydroxyl and carboxyl groups) for mercury binding than other adsorbents (G-HTC and G-PYR). It is also clear that G-HTC outperformed G-PYR because of its higher acidic functional group content. These findings agreed with those reported in the literature regarding the importance of oxygenated functional groups for heavy metal adsorption from water (Arias-Arias *et al.* 2017; Othmani *et al.* 2021). On the other hand, it was found that that the leaching of trace elements (e.g., Mg, Fe, Ca, K, Na) from adsorbent surface did not occur in the aqueous solution after mercury removal.

Table 1 | Chemical and textural properties of carbon-based adsorbents prepared from pyrolysis and hydrothermal carbonization of jacaranda fruit and guava seeds

	Total groups, mmol/g			Textural properties	
Adsorbent	***Basic***	***Acidic***	**pH_{pzc}**	**BET surface area, m^2/g**	**Pore size, Å**
G-PYR	6.70 ± 0.14	9.41 ± 0.10	7.13 ± 0.13	3.4	15.84
G-HTC	6.49 ± 0.11	9.52 ± 0.09	6.30 ± 0.12	<1	8.75
J-PYR	6.43 ± 0.08	9.53 ± 0.07	5.08 ± 0.23	2.4	57.48
J-HTC	6.32 ± 0.13	10.16 ± 0.08	6.28 ± 0.08	<1	9.66

The four adsorbents exhibited different pH_{pzc} values ranging from 5.08 (J-PYR) to 7.13 (G-PYR), see Table 1. At tested solution pH, all the adsorbents were positively charged, and the mercury adsorption capacity of the tested adsorbents decreased as pH_{pzc} increased. This trend indicated that electrostatic forces were a minor contributor to the interaction forces during the removal of this metal cation. The corresponding speciation diagram shows that $HgCl_2$ was mainly present in the aqueous solution at pH 4 (see Supplementary material, Figure S2), thus explaining the negligible effect of the electrostatic forces on the adsorption mechanism. $HgCl_2$ can interact with the acidic functional groups (mainly hydroxyl and carboxyl groups) of these adsorbents via ligand exchange, as described below (Arias-Arias *et al.* 2017; Kaveh & Bagherzadeh 2022). All adsorbents showed specific surface areas < 10 m^2/g and could be classified as low-porosity materials, see Table 1. These results indicated that the surface area of these adsorbents did not play a relevant role for mercury adsorption, which was confirmed with a statistical analysis. Consequently, it could be expected that the interfacial phenomenon for the separation of mercury from the aqueous solution occurred mainly via the interaction with the functional groups located on the external surface of these adsorbents, with a very limited contribution from intraparticle diffusion.

The steric parameters calculated for mercury removal using the tested adsorbents are listed in Table 2. Statistical physics calculations indicated that the adsorption of this toxic metal was multi-molecular, and up to two $HgCl_2$ molecules could interact with each oxygenated functional group on the adsorbent surface. Specifically, n_{Hg} values were 1.9–2.0, 1.6–2.3, 2.0–2.5 and 1.3–2.4 for G-PYR, G-HTC, J-PYR and J-HTC, respectively. The calculated concentrations of adsorption sites involved in the binding of mercury species were 2.41–5.22, 2.41–8.22, 8.02–15.04 and 7.22–14.64 mg/g for G-PYR, G-HTC, J-PYR and J-HTC, respectively. These results indicated that less than 1% of the acidic functional groups available on the adsorbent surface interacted with and adsorbed this heavy metal. The modeling results and textural parameters listed in Table 1 are the basis for inferring that the mercury adsorption occurred mainly on the external surfaces of these adsorbents. The calculated interaction energies ranged from 16 to 20 kJ/mol, confirming that physical interaction forces were responsible of the mechanism of mercury adsorption for these adsorbents. Finally, the calculated saturation adsorption capacities followed the trend: J-PYR (18.05–30.09 mg/g) > J-HTC (10.03–18.05 mg/g) > G-HTC (6.02–14.04 mg/g) > G-PYR (4.01–10.03 mg/g), see Figure 2. J-PYR adsorbent can outperform mercury removal properties reported for other activated carbons and chars obtained via pyrolysis of different lignocellulosic biomass (Hadi *et al.* 2015; Zúñiga-Muro *et al.* 2020; Valdés-Rodríguez *et al.* 2022). In fact, the adsorption properties of J-PYR were better

Table 2 | Results of monolayer statistical physics model for mercury adsorption using carbon-based adsorbents

Adsorbent	T, °C	n_{Hg}	N_{ads}, mg/g	R^2
G-PYR	20	2.0	2.41	0.995
	30	1.9	3.21	0.995
	40	2.0	5.22	0.996
G-HTC	20	2.3	2.41	0.998
	30	1.8	4.01	0.996
	40	1.6	8.22	0.988
J-PYR	20	2.3	8.02	0.993
	30	2.5	9.63	0.997
	40	2.0	15.04	0.999
J-HTC	20	1.3	7.22	0.986
	30	1.3	8.42	0.993
	40	1.3	14.64	0.977

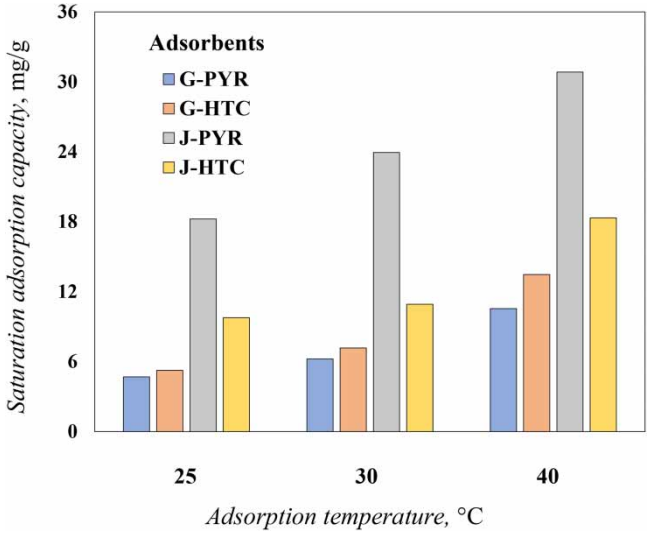

Figure 2 | Calculated saturation adsorption capacities of the carbon-based adsorbents for mercury removal at pH 4.

than those of carbon-based adsorbents prepared by activation with H_2O, H_2SO_4, HCl, H_2O_2, and air, with surface areas of 280–870 m^2/g (Hadi *et al.* 2015). For illustration, Table 3 reports a comparison of the mercury adsorption capacities reported for different materials. The adsorbents obtained from jacaranda fruit and guava seed biomass showed reasonable removal performance in comparison with other biomass-based adsorbents, although they were outperformed by silicon-based materials such as SBA-15 and MCM-41. However, it is important to highlight that the carbon-based materials prepared from residual biomass and its subproducts usually offer more benefits in terms of environmental protection, low production cost, biomass waste minimization and final disposal.

3.2. Physicochemical characterization of carbon-based adsorbents used in mercury removal

XRD diffractograms of the four adsorbents with and without loaded mercury are shown in Figure 3. All samples showed the characteristic patterns of carbon-based materials derived from lignocellulosic biomass. Specifically, the XRD patterns of J-HTC and G-HTC contained wide diffraction peaks at ~ 15°, 22°, and 34° 2θ, attributed to cellulose crystallization (Wang *et al.* 2022), as shown in Figure 3(a). This result indicated that only a fraction of biomass cellulose was converted during the hydrothermal reaction (Han *et al.* 2017; Li *et al.* 2021). However, the diffraction peaks of the cellulose crystals disappeared in the diffraction pattern of the pyrolysis-based adsorbents (Figure 3(b)), leading to the formation of carbon planes characteristic of graphitic structures, which

Table 3 | Mercury adsorption capacities reported for different adsorbents

Adsorbent	pH	Temperature, °C	Adsorption capacity, mg/g	Reference
Activated carbon from beer barley husk	6	25	109.37	Gheitasi *et al.* (2022)
Activated carbon from grape pomace	4	25	4.21	Valdés-Rodríguez *et al.* (2022)
Activated carbon from guava seeds			61.18	
Activated carbon from *J. mimosifolia* seeds			130.58	
Activated carbon from sugarcane bagasse			104.71	
Biochar from rice straw biogas residue	4	25	209.65	Liu *et al.* (2022)
Grape bagasse-based char	4	30	32.29	Zúñiga-Muro *et al.* (2020)
Corn husk biomass	6	25	18.86	Núñez-Zarur *et al.* (2018)
Spanish broom plant	5	-	19.86	Arias-Arias *et al.* (2017)
Coconut pit char	4.5	30	46.14	Saman *et al.* (2016)
Activated carbon from coconut pit			142.42	
Candlenut shell charcoal	–	25	76.35	Mariana *et al.* (2022)
Candlenut shell particles			37.18	
Magnetic rice straw-derived biochar	5	25	~73.00	Lim *et al.* (2023)
Magnetic activated carbon	7	–	166.60	Kaveh & Bagherzadeh (2022)
Thiol functionalized SBA-15	8	25	~225.00	Shen *et al.* (2018)
SBA-15/Ag nanocomposite	7	27	42.26	Ganzagh *et al.* (2016)
MCM-41 modified by $ZnCl_2$	6	20	87.00	Raji & Pakizeh (2014)
Amine-grafted MCM-41	6	25	118.35	Zhu *et al.* (2012)
β-cyclodextrin/MCM-48 composite	6	20	173.40	Jumah *et al.* (2021)
Guava seed hydrochar (G-HTC)	4	30	6.88	This study
Jacaranda hydrochar (J-HTC)			10.38	
Guava seed char (G-PYR)			5.82	
Jacaranda char (J-PYR)			23.47	

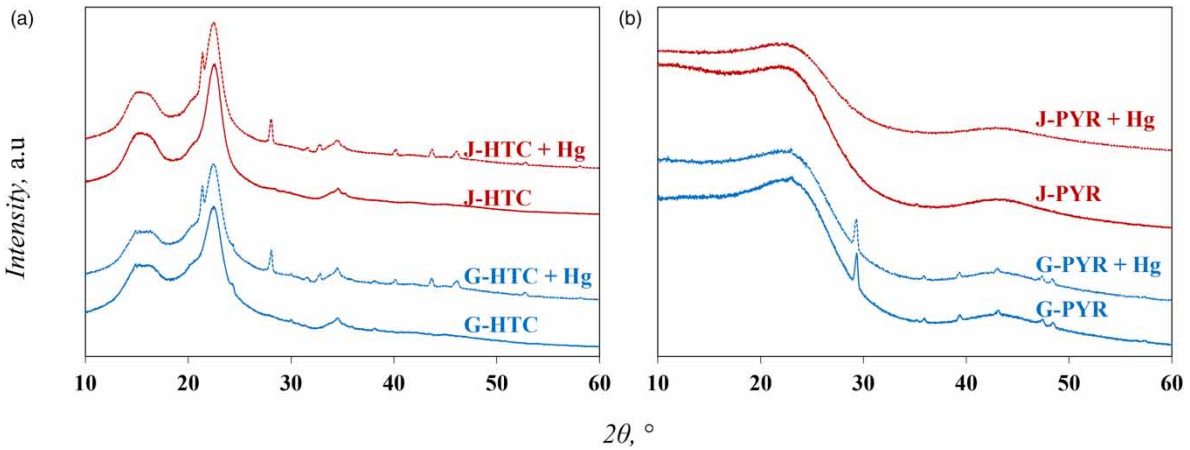

Figure 3 | X-ray diffraction patterns of carbon-based adsorbents synthesized from jacaranda fruits and guava seeds biomass using (a) hydrothermal carbonization and (b) pyrolysis. Label '+ Hg' indicates the adsorbent samples loaded with mercury

corresponded to the two diffraction peaks at ~22° and 43° 2θ (Nanda *et al.* 2012; Li *et al.* 2021; Pan *et al.* 2021; He *et al.* 2023). The amorphous behavior of these samples suggested that the microcrystalline structure of cellulose was destroyed (Han *et al.* 2017). This result was associated with the thermal treatment conditions and

degradation temperatures of the structural biopolymers (i.e., cellulose, hemicellulose, and lignin) contained in both precursors (Heidari *et al.* 2019; Li *et al.* 2020; Pan *et al.* 2021). Other diffraction peaks at ~29.3°, 35.9°, 39.4°, 43.2°, 47.4°, and 48.4° 2θ corresponding to the crystalline structure of calcium carbonate (ICDD: 00-005-0586) were identified in the G-PYR sample. Calcium is a component of the mineral composition of guava seeds, including iron, copper, zinc, magnesium, and other trace elements (Pezoti *et al.* 2016; Silveira-Junior *et al.* 2020). After the loading of mercury on the adsorbent surfaces, a decrease in the crystallinity of all samples was observed. This change in the diffraction patterns was caused by the incorporation of this heavy metal on the adsorbent surface (Marciniak *et al.* 2019; Li *et al.* 2020). New diffraction peaks (at ~21.4°, 28.1°, 31.6°, 32.8°, 40.2°, 43.7°, 46.1°, and 52.8° 2θ) associated with mercury chloride (ICDD: 01-073-1247) were identified in the XRD results of the adsorbent samples that were synthesized via hydrothermal carbonization. Note that analogous results were reported by Liu *et al.* (2022). The interaction between mercury and the main oxygenated functional groups of carbon-based adsorbents can imply a ligand exchange, which is represented as follows (Chaudhuri *et al.* 2022)

$$-\mathrm{OH} + \mathrm{HgCl_2} \rightarrow -\mathrm{OHgCl_2} + \mathrm{H^+} \quad (8)$$

$$-\mathrm{COOH} + \mathrm{HgCl_2} \rightarrow -\mathrm{COOHgCl_2} + \mathrm{H^+} \quad (9)$$

In addition, van der Waals forces may have been present during the mercury adsorption (Lim *et al.* 2023).

As stated, the surface area of tested adsorbents was $<10\ \mathrm{m^2/g}$ for all samples and, consequently, they can be considered as low-porosity adsorbents. On the other hand, Figure 4 shows the surface morphologies at 100x of the four carbon-based adsorbents synthesized from jacaranda fruit and guava seed biomass. The adsorbents prepared by hydrothermal carbonization exhibited a rough, compact, and irregular morphology with low porosity. In contrast, the J-PYR and G-PYR adsorbents had irregular cavities with different shapes and sizes owing to the surface breakage and fragmentation of large to small molecules during thermal treatment (Treviño-Cordero *et al.* 2013; Basu 2018; Pan *et al.* 2021). Elemental analysis indicated that all adsorbents were mainly composed of oxygen (4–25%) and carbon (75–95%), which are the main elements in lignocellulosic-based materials (Treviño-Cordero *et al.* 2013; Mendoza-Castillo *et al.* 2014).

FTIR spectra of all adsorbent samples are given in Figure 5. The absorption band of the stretching vibration of the hydrogen bonded to the –OH group identified at ~3,420 $\mathrm{cm^{-1}}$ was due to alcohols linked to the polymeric

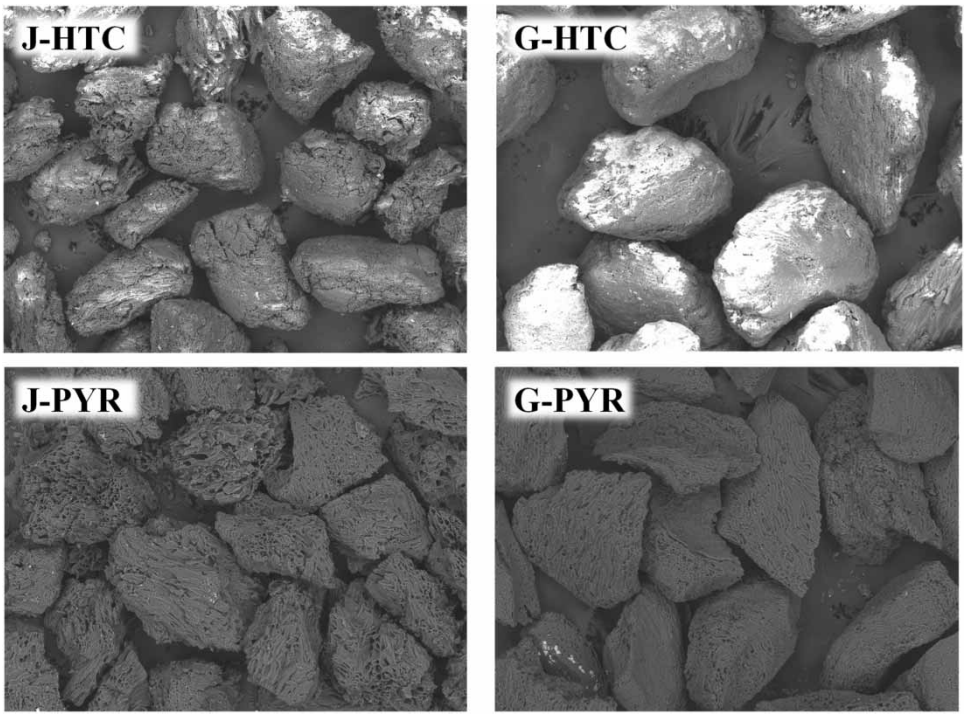

Figure 4 | SEM micrographs of carbon-based adsorbents synthesized from jacaranda fruits and guava seeds biomass by hydrothermal carbonization and pyrolysis.

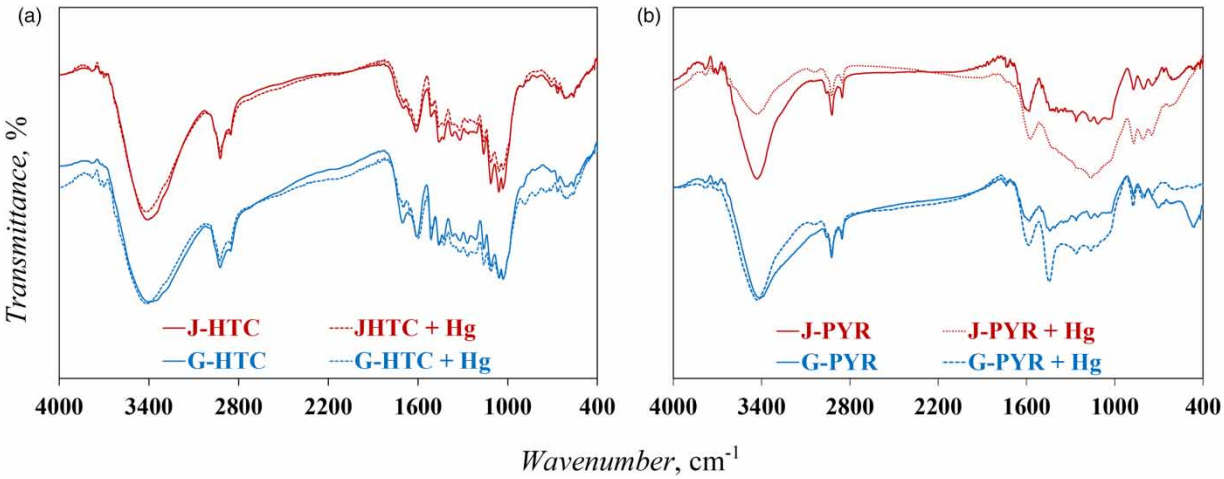

Figure 5 | FTIR spectra of carbon-based adsorbents synthetized from jacaranda fruits and guava seeds biomass using (a) hydrothermal carbonization and (b) pyrolysis. Label '+ Hg' indicates the adsorbent samples loaded with mercury.

content of the biomass precursor (Lima *et al.* 2007; Li *et al.* 2018, 2020; Mamaní *et al.* 2019; Yoo *et al.* 2023). The absorption bands at ~2,930–2,850 cm^{-1} corresponded to the C–H stretching vibrations of aliphatic chains (Li *et al.* 2018, 2020; Mamaní *et al.* 2019). The set of absorption bands located between ~2,000 and 1,500 cm^{-1} were associated with the C = C stretching vibration (~1,600 cm^{-1}) present in the aromatic rings and the C = O stretching vibration (~1,700 and 1,435 cm^{-1}) of the carboxylic groups, respectively (Lima *et al.* 2007; Li *et al.* 2018, 2020; Mamaní *et al.* 2019). The absorption bands at approximately 1,300–910 cm^{-1} were assigned to the C–O stretching vibrations of carbonyls, alcohols, carboxylic acids, phenols, ethers, and esters (Li *et al.* 2018, 2020; Mamaní *et al.* 2019), whereas the absorption bands at ~870–700 cm^{-1} originated from the out-of-plane deformation produced by aromatic C-H atoms (Zhang *et al.* 2023b). FTIR spectra of the adsorbents synthetized via hydrothermal carbonization differed significantly than those of adsorbents prepared by pyrolysis. The absorption bands of some functional groups lose their intensity, indicating that their degradation was caused by the temperature used in the thermochemical conversion of the precursor (Sun *et al.* 2021). FTIR spectra of the mercury-loaded adsorbents showed a change in the intensity of absorption bands of the carboxyl and hydroxyl groups, indicating the contribution of these oxygenated functionalities during mercury adsorption (Mamaní *et al.* 2019; Sellaoui *et al.* 2019). Similar findings have been reported by Yoo *et al.* (2023), Goyal *et al.* (2009), Guo *et al.* (2020) and Zhao *et al.* (2022). The most significant changes were observed in the FTIR spectra of the pyrolysis-based adsorbents (i.e., J-PYR and G-PYR samples).

4. CONCLUSIONS

The mercury adsorption properties of adsorbents prepared from hydrothermal carbonization and pyrolysis of jacaranda and guava seed wastes were analyzed and compared. Mercury adsorption on these adsorbents was endothermic and may involve a multi-molecular interaction mechanism with oxygenated functionalities. van der Waals and ligand exchange are expected to be the main interaction forces for the mercury adsorption mechanism using these adsorbents. The carbon-based materials obtained from jacaranda exhibited the highest mercury adsorption capacities where the biomass pyrolysis allowed to obtain the adsorbent with the best mercury removal. This adsorbent outperformed the adsorption capacities of other activated carbons with higher surface areas. It was expected that the mercury adsorption on these carbon-based materials occurred mainly on their external surface with a limited contribution from intraparticle diffusion. The lignin content of jacaranda waste favored the formation of oxygenated functionalities during biomass thermochemical conversion, especially pyrolysis, under the tested experimental conditions.

ACKNOWLEDGEMENTS

The support provided by the MatPore – Porous Materials National Laboratory is acknowledged.

AUTHORS CONTRIBUTIONS

All authors contributed to the study conception and design. V.A.M.-H., F.G.Q.-Á., D.I.M.-C., and A.B.-P. conceptualized the study; V.A.M.-H., F.G.Q.-Á., D.I.M.-C., H.E.R.-Á., I.A.A.-V., and A.B.-P. performed the methodology; F.G.Q.-Á., H.E.R.-Á., D.I.M.-C., H.E.R.-Á., I.A.A.-V., V.J.L.-S., and A.B.-P. investigated the study; F.G.Q.-Á., H.E.R.-Á., I.A.A.-V., and D.I.M.-C. wrote and prepared the original draft; D.I.M.-C. and A.B.-P. wrote, reviewed, and edited the article; D.I.M.-C. supervised the study; D.I.M.-C. did project administration . All the authors have read and agreed to the published version of the manuscript.

FUNDING

This research received no external funding.

DATA AVAILABILITY STATEMENT

All relevant data are included in the paper or its Supplementary Information.

CONFLICT OF INTEREST

The authors declare there is no conflict.

REFERENCES

Abdelwahab, O., El Sikaily, A., Khaled, A. & El Nemr, A. 2007 Mass-transfer processes of chromium (VI) adsorption onto guava seeds. *Chemistry and Ecology* **23**, 73–85.

Ali, N. S., Kalash, K. R., Ahmed, A. N. & Albayati, T. M. 2022a Performance of a solar photocatalysis reactor as pretreatment for wastewater via UV, UV/TiO2, and UV/H2O2 to control membrane fouling. *Scientific Reports* **12**, 16782.

Ali, A. E., Mustafa, A. A., Eledkawy, M. A., Ahmed, A. M., Alnaggar, G. A., Elmelegy, E. & Kolkaila, S. 2022b Removal of cadmium (II) from water by adsorption on natural compound. *Journal of Environmental Treatment Techniques* **10**, 164–169.

Al-Jaaf, H. J., Ali, N. S., Alardhi, S. M. & Albayati, T. M. 2022 Implementing eggplant peels as an efficient bio-adsorbent for treatment of oily domestic wastewater. *Desalination Water Treatment* **245**, 226–237.

Aly, S. T., El-Sayed, A. M., Tharwat, K. M., Mahmoud, M. A., Khaled, A. M., Gad, A. M. & Mahmoud, A. T. 2019 Adsorption of Nile blue dye using guava leaf powder. *International Journal of Engineering Research & Technology* **8**, 69–72.

Amrhar, O., El Gana, L. & Mobarak, M. 2021 Calculation of adsorption isotherms by statistical physics models: A review. *Environmental Chemistry Letters* **19**, 4519–4547.

Anisuzzaman, S. M., Joseph, C. G., Krishnaiah, D., Bono, A., Suali, E., Abang, S. & Fai, L. M. 2016 Removal of chlorinated phenol from aqueous media by guava seed (*Psidium guajava*) tailored activated carbon. *Water Resources and Industry* **16**, 29–36.

Arias-Arias, F. E., Beneduci, A., Chidichimo, F., Furia, E. & Straface, S. 2017 Study of the adsorption of mercury (II) on lignocellulosic materials under static and dynamic conditions. *Chemosphere* **180**, 11–23.

Basu, P. 2018 Chapter 5 – Pyrolysis. In: *Biomass Gasification, Pyrolysis and Torrefaction: Practical Design and Theory*, Vol. 3. Academic Press, San Diego, USA, pp. 155–187.

Behera, U. S., Mishra, P. C. & Radhika, G. B. 2022 Optimization of multiple parameters for adsorption of arsenic (III) from aqueous solution using *Psidium guajava* leaf powder. *Water Science & Technology* **85**, 515–534.

Beri, K. Y. V., Barbosa, D. P., Zbair, M., Ojala, S. & de Oliveira, S. B. 2021 Adsorption of estradiol from aqueous solution by hydrothermally carbonized and steam activated palm kernel shells. *Energy Nexus* **1**, 100009.

Boehm, H. P. 1994 Some aspects of the surface chemistry of carbon blacks and other carbons. *Carbon* **32**, 759–769.

Chaudhuri, S., Sigmund, G., Bone, S. E., Kumar, N. & Hofmann, T. 2022 Mercury removal from contaminated water by wood-based biochar depends on natural organic matter and ionic composition. *Environmental Science & Technology* **56**, 11354–11362.

Correa, C. R., Hehr, T., Rauscher, Y., Alhnidi, M. J. & Kruse, A. 2019 Biomass carbonization-an experimental comparison between pyrolysis and hydrothermal carbonization. *Journal of Analytical and Applied Pyrolysis* **214**, 137–147.

Domínguez, S. J. M. & Serrano, L. S. S. 2004 Procurement of activated carbon from jacaranda (*Mimosifolia*). *International Journal of Engineering Science and Innovative Technology* **3**, 473–478.

Duman, G. 2021 Preparation of novel porous carbon from hydrothermal pretreated textile wastes: Effects of textile type and activation agent on structural and adsorptive properties. *Journal of Water Process Engineering* **43**, 102286.

Elizalde-González, M. P. & Hernández-Montoya, V. 2009 Guava seed as an adsorbent and as a precursor of carbon for the adsorption of acid dyes. *Bioresource Technology* **100**, 2111–2117.

Ganzagh, M. A. A., Yousefpour, M. & Taherian, Z. 2016 The removal of mercury (II) from water by Ag supported on nanomesoporous silica. *Journal of Chemical Biology* **9**, 127–142.

Georgin, J., Salomón, Y. L. O., Franco, D. S. P., Netto, M. S., Piccilli, D. G. A., Perondi, D., Silva, L. F. O., Foletto, E. L. & Dotto, G. L. 2021 Development of highly porous activated carbon from *Jacaranda mimosifolia* seed pods for remarkable removal of aqueous-phase ketoprofen. *Journal of Environmental Chemical Engineering* **9**, 105676.

Gheitasi, F., Ghammamy, S., Zendehdel, M. & Semiromi, F. B. 2022 Removal of mercury(II) from aqueous solution by powdered activated carbon nanoparticles prepared from beer barley husk modified with Thiol/Fe_3O_4. *Journal of Molecular Structure* **1267**, 133555.

Goyal, M., Bhagat, M. & Dhawan, R. 2009 Removal of mercury from water by fixed bed activated carbon columns. *Journal of Hazardous Materials* **171**, 1009–1015.

Guo, X., Li, M., Liu, A., Jiang, M., Niu, X. & Li, X. 2020 Adsorption mechanisms and characteristics of Hg^{2+} removal by different fractions of biochar. *Water* **12**, 2105.

Hadi, P., To, M. H., Hui, C. W., Lin, C. S. K. & McKay, G. 2015 Aqueous mercury adsorption by activated carbons. *Water Research* **73**, 37–55.

Han, M., Jiang, K., Jiao, P., Ji, Y., Zhou, J., Zhuang, W., Chen, Y., Liu, D., Zhu, C., Chen, X., Ying, H. & Wu, J. 2017 Bio-butanol sorption performance on novel porous-carbon adsorbents from corncob prepared via hydrothermal carbonization and post-pyrolysis method. *Scientific Reports* **7**, 11753.

He, L., Qiu, Y., Yao, C., Lan, G., Li, N., Zhou, H., Liu, Q., Sun, X., Cheng, Z. & Li, Y. 2023 Role of intrinsic defects on carbon adsorbent for enhanced removal of Hg^{2+} in aqueous solution. *Chinese Journal of Chemical Engineering* **61**, 129–139.

Heidari, M., Dutta, A., Acharya, B. & Mahmud, S. 2019 A Review of the current knowledge and challenges of hydrothermal carbonization for biomass conversion. *Journal of the Energy Institute* **92**, 1779–1799.

Ismaiel, A. A., Aroua, M. K. & Yusoff, R. 2013 Palm shell activated carbon impregnated with task-specific ionic-liquids as a novel adsorbent for the removal of mercury from contaminated water. *Chemical Engineering Journal* **225**, 306–314.

Jain, A., Balasubramanian, R. & Srinivasan, M. P. 2015 Production of high surface area mesoporous activated carbons from waste biomass using hydrogen peroxide-mediated hydrothermal treatment for adsorption applications. *Chemical Engineering Journal* **273**, 622–629.

Jian, X., Zhuang, X., Li, B., Xu, X., Wei, Z., Song, Y. & Jiang, E. 2018 Comparison of characterization and adsorption of biochars produced from hydrothermal carbonization and pyrolysis. *Environmental Technology & Innovation* **10**, 27–35.

Jumah, M. N. B., Eid, M. H., Al-Huqail, A. A., Mohammad, M. A., Bin-Murdhi, N. S., Abu-Taweel, G. M., Altoom, N., Allam, A. A. & Abukhadra, M. R. 2021 Enhanced remediation of As (V) and Hg (II) ions from aqueous environments using β-cyclodextrin/MCM-48 composite: Batch and column studies. *Journal of Water Process Engineering* **42**, 102118.

Jung, K. W., Lee, S. Y., Choi, J. W., Hwang, M. J. & Shim, W. G. 2021 Synthesis of Mg–Al layered double hydroxides-functionalized hydrochar composite via an in situ one-pot hydrothermal method for arsenate and phosphate removal: Structural characterization and adsorption performance. *Chemical Engineering Journal* **420**, 129775.

Kaveh, R. & Bagherzadeh, M. 2022 Simultaneous removal of mercury ions and cationic and anionic dyes from aqueous solution using epichlorohydrin cross-linked chitosan @ magnetic Fe_3O_4/activated carbon nanocomposite as an adsorbent. *Diamond and Related Materials* **124**, 108923.

Li, X., Wei, Y., Xu, J., Xu, N. & He, Y. 2018 Quantitative visualization of lignocellulose components in transverse sections of moso bamboo based on FTIR macro- and micro-spectroscopy coupled with chemometrics. *Biotechnology for Biofuels* **11**, 263.

Li, F., Zimmerman, A. R., Hu, X., Yu, Z., Huang, J. & Gao, B. 2020 One-pot synthesis and characterization of engineered hydrochar by hydrothermal carbonization of biomass with $ZnCl_2$. *Chemosphere* **254**, 126866.

Li, M., Zhang, S., Cui, S., Qin, K., Zhang, Y., Li, P., Cao, Q., Xiao, H. & Zeng, Q. 2021 Pre-grafting effect on improving adsorption efficiency of cellulose based biosorbent for Hg(II) removal from aqueous solution. *Separation and Purification Technology* **277**, 119493.

Lim, Y., Kim, B., Jang, J. & Lee, D. S. 2023 Magnetic rice-straw-derived biochar for adsorptive removal of Hg(II) from aqueous solution: Optimization using response surface methodology. *Journal of Environmental Chemical Engineering* **11**, 110048.

Lima, E. C., Royer, B., Vaghetti, J. C. P., Brasil, J. L., Simon, N. M., dos Santos, A. A., Pavan, F. A., Dias, S. L. P., Benvenutti, E. V. & da Silva, E. A. 2007 Adsorption of Cu(II) on *Araucaria angustifolia* wastes: Determination of the optimal conditions by statistic design of experiments. *Journal of Hazardous Materials* **140**, 211–220.

Lima, E. C., Gomes, A. A. & Tran, H. N. 2020 Comparison of the nonlinear and linear forms of the van't Hoff equation for calculation of adsorption thermodynamic parameters $\Delta S°$ and $\Delta H°$. *Journal of Molecular Liquids* **311**, 113315.

Liu, Z., Zhen, F., Zhang, Q., Qian, X., Li, W., Sun, Y., Zhang, L. & Qu, B. 2022 Nanoporous biochar with high specific surface area based on rice straw digestion residue for efficient adsorption of mercury ion from water. *Bioresource Technology* **359**, 127471.

Luo, X., Huang, Z., Lin, J., Li, X., Qiu, J., Liu, J. & Mao, X. 2020 Hydrothermal carbonization of sewage sludge and in-situ preparation of hydrochar/MgAl-layered double hydroxides composites for adsorption of Pb(II). *Journal of Cleaner Production* **258**, 120991.

Mamaní, A., Ramírez, N., Deiana, C., Giménez, M. & Sardella, F. 2019 Highly microporous sorbents from lignocellulosic biomass: Different activation routes and their application to dyes adsorption. *Journal of Environmental Chemical Engineering* **7**, 103148.

Mandal, A., Mukhopadhyay, P. & Das, S. K. 2020 Adsorptive removal of phenol from wastewater using guava tree bark. *Environmental Science and Pollution Research* **27**, 23937–23949.

Marciniak, M., Goscianska, J., Frankowski, M. & Pietrzak, R. 2019 Optimal synthesis of oxidized mesoporous carbons for the adsorption of heavy metal ions. *Journal of Molecular Liquids* **276**, 630–637.

Mariana, M., Mistar, E. M., Syabriyana, M., Zulkipli, A. S., Aswita, D. & Alfatah, T. 2022 Properties and adsorptive performance of candlenut shell and its porous charcoals for aqueous mercury(II) removal. *Bioresource Technology Reports* **19**, 101182.

Mendoza-Castillo, D. I., Villalobos-Ortega, N., Bonilla-Petriciolet, A. & Tapia-Picazo, J. C. 2014 Neural network modeling of heavy metal sorption on lignocellulosic biomasses: Effect of metallic ion properties and sorbent characteristics. *Industrial & Engineering Chemistry Research* **54**, 443–453.

Milonjić, S. K., Ruvarac, A. L. & Šušić, M. V. 1975 The heat of immersion of natural magnetite in aqueous solutions. *Thermochimica Acta* **11**, 261–266.

Mohan, D., Dey, S., Dwivedi, S. B. & Shukla, S. P. 2019 Adsorption of arsenic using low cost adsorbents: Guava leaf biomass, mango bark and bagasse. *Current Science* **117**, 649–661.

Nanda, S., Mohanty, P., Pant, K. K., Naik, S., Kozinski, J. A. & Dalai, A. K. 2012 Characterization of North American lignocellulosic biomass and biochars in terms of their candidacy for alternate renewable fuels. *BioEnergy Research* **6**, 663–677.

Nguyen, J. T. B., Truong, Q. M., Chen, C. W., Doong, R., Chen, W. H. & Dong, C. D. 2022 Mesoporous and adsorption behavior of algal biochar prepared via sequential hydrothermal carbonization and $ZnCl_2$ activation. *Bioresource Technology* **346**, 126351.

Núñez-Zarur, J., Tejada-Tovar, C., Villabona-Ortíz, A., Acevedo, D. & Tejada-Tovar, R. 2018 Thermodynamics, kinetics and equilibrium adsorption of Cr (VI) and Hg (II) in aqueous solution on corn husk (*Zea Mays*). *International Journal of ChemTech Research* **11**, 265–280.

Ortíz-Gutiérrez, M., Cuevas-Villanueva, R. A., Martínez-Miranda, V., Hernández-Cristóbal, O. & Cortés-Martínez, R. 2020 Reduction and biosorption of Cr (VI) from aqueous solutions by acid-modified guava seeds: Kinetic and equilibrium studies. *Polish Journal of Chemical Technology* **22**, 36–47.

Othmani, A., John, J., Rajendran, H., Mansouri, A., Sillanpää, M. & Chellam, P. V. 2021 Biochar and activated carbon derivatives of lignocellulosic fibers towards adsorptive removal of pollutants from aqueous systems: Critical study and future insight. *Separation and Purification Technology* **274**, 119062.

Pan, H., Sun, J., Liu, J., Zhang, Y. & Zhou, S. 2021 Preparation of sulfonated carbon derived from orange peel and its application in esterification. *Chemical Physics Letters* **770**, 138395.

Park, J. H., Wang, J. J., Zhou, B., Mikhael, J. E. R. & Laune, R. D. D. 2019 Removing mercury from aqueous solution using sulfurized biochar and associated mechanisms. *Environmental Pollution* **244**, 627–635.

Pawlicka, A. & Doczekalska, B. 2013 Determination of surface oxygen functional groups of active carbons according to the Boehm's titration method. *Forestry and Wood Technology* **84**, 11–14.

Pezoti, O., Cazetta, A. L., Bedin, K. C., Souza, L. S., Martins, A. C., Silva, T. L., Santos Júnior, O. O., Visentainer, J. V. & Almeida, V. C. 2016 NaOH-activated carbon of high surface area produced from guava seeds as a high-efficiency adsorbent for amoxicillin removal: Kinetic, isotherm and thermodynamic studies. *Chemical Engineering Journal* **288**, 778–788.

Pindiga, N. Y., Walid, A. H., Abdullahi, A. O. & Mohammad, A. B. 2022 Kinetic, equilibrium and thermodynamic study of the adsorption of Pb (II) and Cd (II) ions from aqueous solution by the leaves biomass of guava and cashew plants. *Online Journal of Chemistry* **2**, 23–38.

Plavniece, A., Dobele, G., Volperts, A. & Zhurinsh, A. 2022 Hydrothermal carbonization vs. pyrolysis: effect on the porosity of the activated carbon materials. *Sustainability* **14**, 15982.

Prasetya, A., Prihutami, P., Warisaura, A. D., Fahrurrozi, M. & Petrus, H. T. B. M. 2020 Characteristic of Hg removal using zeolite adsorption and *Echinodorus palaefolius* phytoremediation in subsurface flow constructed wetland (SSF-CW) model. *Journal of Environmental Chemical Engineering* **8**, 103781.

Qin, S., Wang, C., Jia, L., Fan, B., Wang, Y., Qiao, X., Guo, B. & Jin, Y. 2023 Study on mercury adsorption mechanism of iron-modified biomass char in coal-fired flue gas based on density functional theory. *Fuel Processing Technology* **247**, 107801.

Raji, F. & Pakizeh, M. 2014 Kinetic and thermodynamic studies of Hg(II) adsorption onto MCM-41 modified by $ZnCl_2$. *Applied Surface Science* **301**, 568–575.

Rattanachueskul, N., Saning, A., Kaowphong, S., Chumha, N. & Chuenchom, L. 2017 Magnetic carbon composites with a hierarchical structure for adsorption of tetracycline, prepared from sugarcane bagasse via hydrothermal carbonization coupled with simple heat treatment process. *Bioresource Technology* **226**, 164–172.

Rodríguez-Correa, C., Hehr, T., Voglhuber-Slavinsky, A., Rauscher, Y. & Kruse, A. 2019 Pyrolysis vs. hydrothermal carbonization: Understanding the effect of biomass structural components and inorganic compounds on the char properties. *Journal of Analytical and Applied Pyrolysis* **140**, 137–147.

Saman, N., Johari, K., Song, S. T., Kong, H., Cheu, S. C. & Mat, H. 2016 High removal efficiency of Hg(II) and MeHg(II) from aqueous solution by coconut pith – equilibrium, kinetic and mechanism analyses. *Journal of Environmental Chemical Engineering* **4**, 2487–2499.

Sánchez-Sánchez, H. A., Cortés-Martínez, R. & Cuevas-Villanueva, R. A. 2013 Fluoride removal from aqueous solutions by mechanically modified guava seeds. *International Journal of Sciences: Basic and Applied Research* **11**, 159–172.

Sellaoui, L., Mendoza-Castillo, D. I., Reynel-Ávila, H. E., Ávila-Camacho, B. A., Díaz-Muñoz, L. L., Ghalla, H., Bonilla-Petriciolet, A. & Lamine, A. B. 2019 Understanding the adsorption of Pb^{2+}, Hg^{2+} and Zn^{2+} from aqueous solution on a lignocellulosic biomass char using advanced statistical physics models and density functional theory simulations. *Chemical Engineering Journal* **365**, 305–316.

Shen, Y., Jiang, N., Liu, S., Zheng, C., Wang, X., Huang, T., Guo, Y. & Bai, R. 2018 Thiol functionalization of short channel SBA-15 through a safe, mild and facile method and application for the removal of mercury (II). *Journal of Environmental Chemical Engineering* **6**, 5420–5433.

Shukla, P., Manivannan, S. & Mandal, D. 2023 Silver zeolite in ultrasonically welded packed beds for enhanced elemental mercury capture from contaminated air stream: Adsorption and kinetics study. *Microporous and Mesoporous Materials* **359**, 112651.

Silveira-Junior, E. G., Perez, V. H., Rodriguez-Justo, O., Ferreira-David, G., Simionatto, E. & Silva de Oliveira, L. C. 2020 Valorization of guava (*Psidium guajava L.*) seeds for levoglucosan production by fast pyrolysis. *Cellulose* **28**, 71–79.

Sun, L., Chen, T., Ba, C., Rein, T. R. & Yu, J. 2021 Preparation of sorbents derived from bamboo and bromine flame retardant for elemental mercury removal. *Journal of Hazardous Materials* **410**, 124583.

Syversen, T. & Kaur, P. 2012 The toxicology of mercury and its compounds. *Journal of Trace Elements in Medicine and Biology* **26**, 215–226.

Tran, H. N., You, S. J., Hosseini-Bandegharaei, A. & Chao, H. P. 2017 Mistakes and inconsistencies regarding adsorption of contaminants from aqueous solutions: A critical review. *Water Research* **120**, 88–116.

Tran, H. V., Hoang, L. T. & Huynh, C. D. 2020 An investigation on kinetic and thermodynamic parameters of methylene blue adsorption onto graphene-based nanocomposite. *Chemical Physics* **535**, 110793.

Tran, T. H., Le, H. H., Pham, T. H., Nguyen, D. T., La, D. D., Chang, S. W., Lee, S. M., Chung, W. J. & Nguyen, D. D. 2021 Comparative study on methylene blue adsorption behavior of coffee husk-derived activated carbon materials prepared using hydrothermal and soaking methods. *Journal of Environmental Chemical Engineering* **9**, 105362.

Treviño-Cordero, H., Juárez-Aguilar, L. G., Mendoza-Castillo, D. I., Hernández-Montoya, V., Bonilla-Petriciolet, A. & Montes-Morán, M. A. 2013 Synthesis and adsorption properties of activated carbons from biomass of *Prunus domestica* and *Jacaranda mimosifolia* for the removal of heavy metals and dyes from water. *Industrial Crops and Products* **42**, 315–323.

Valdés-Rodríguez, E. M., Mendoza-Castillo, D. I., Reynel-Ávila, H. E., Aguayo-Villarreal, I. A. & Bonilla-Petriciolet, A. 2022 Activated carbon manufacturing via alternative Mexican lignocellulosic biomass and their application in water treatment: Preparation conditions, surface chemistry analysis and heavy metal adsorption properties. *Chemical Engineering Research and Design* **187**, 9–26.

Valencia-Leal, S. A., Cortés-Martínez, R. & Alfaro-Cuevas-Villanueva, R. 2012 Evaluation of guava seeds (*Psidium guajava*) as a low-cost biosorbent for the removal of fluoride from aqueous solutions. *International Journal of Engineering Research and Development* **5**, 69–76.

Velempini, T. & Pillay, K. 2019 Sulphur functionalized materials for Hg(II) adsorption: A review. *Journal of Environmental Chemical Engineering* **7**, 103350.

Wang, J., Wang, Y., Wang, J., Du, G., Khan, K. Y., Song, Y., Cui, X., Cheng, Z., Yan, B. & Chen, G. 2022 Comparison of cadmium adsorption by hydrochar and pyrochar derived from Napier grass. *Chemosphere* **308**, 136389.

Yang, G., Song, S., Li, J., Tang, Z., Ye, J. & Yang, J. 2019 Preparation and CO_2 adsorption properties of porous carbon by hydrothermal carbonization of tree leaves. *Journal of Materials Science and Technology* **35**, 875–884.

Yoo, S. H., Lee, S. C., Ko, M., Yoon, S., Lee, J., Park, J. A. & Kim, S. B. 2023 Adsorption of Hg(II) on polyethyleneimine-functionalized carboxymethylcellulose beads: Characterization, toxicity tests, and adsorption experiments. *International Journal of Biological Macromolecules* **241**, 124516.

Zabihi, M., Asl, A. H. & Ahmadpour, A. 2010 Studies on adsorption of mercury from aqueous solution on activated carbons prepared from walnut shell. *Journal of Hazardous Materials* **174**, 251–256.

Zhang, T., Zhang, J., Wei, S., Xiong, Z., Xiao, R., Chuai, X. & Zhao, Y. 2023a Effect of hydrothermal pretreatment on mercury removal performance of modified biochar prepared from corn straw. *Fuel* **339**, 126958.

Zhang, Y., Hu, J., Cheng, X. & Tahir, M. H. 2023b Pyrolysis characteristics, kinetics, and biochar of fermented pine sawdust–based waste. *Environmental Science and Pollution Research* **30**, 39994–40007.

Zhao, S., Luo, H., Ma, A., Xie, W., Sun, K. & Sun, Z. 2022 Influence of pyrolysis conditions on the mercury removal characteristics and physicochemical properties of biomass coke. *Fuel* **313**, 122979.

Zhu, Z., Yang, X., He, L. N. & Li, W. 2012 Adsorption of Hg^{2+} from aqueous solution on functionalized MCM-41. *RSC Advances* **2**, 1088–1095.

Zúñiga-Muro, N. M., Bonilla-Petriciolet, A., Mendoza-Castillo, D. I., Reynel-Ávila, H. E., Duran-Valle, C. J., Ghalla, H. & Sellaoui, L. 2020 Recovery of grape waste for the preparation of adsorbents for water treatment: Mercury removal. *Journal of Environmental Chemical Engineering* **8**, 103738.

First received 18 September 2023; accepted in revised form 16 February 2024. Available online 4 March 2024